Lab on a Chip

PAPER

View Article Online
View Journal | View Issue

Cite this: *Lab Chip*, 2016, **16**, 1466

A microfluidic array for real-time live-cell imaging of human and rodent pancreatic islets†

Mohammad Nourmohammadzadeh,[ab] Yuan Xing,[ab] Jin Wuk Lee,[c] Matthew A. Bochenek,[ab] Joshua E. Mendoza-Elias,[ab] James J. McGarrigle,[a] Enza Marchese,[a] Yeh Chun-Chieh,[a] David T. Eddington,[b] José Oberholzer*[ab] and Yong Wang*[ab]

Received 29th September 2015,
Accepted 4th March 2016

DOI: 10.1039/c5lc01173f

www.rsc.org/loc

In this study, we present a microfluidic array for high-resolution imaging of individual pancreatic islets. The device is based on hydrodynamic trapping principle and enables real-time analysis of islet cellular responses to insulin secretagogues. This device has significant advantages over our previously published perifusion chamber device including significantly increased analytical power and assay sensitivity, as well as improved spatiotemporal resolution. The islet array, with live-cell multiparametric imaging integration, provides a better tool to understand the physiological and pathophysiological changes of pancreatic islets through the analysis of single islet responses. This platform demonstrates the feasibility of array-based islet cellular analysis and opens up a new modality to conduct informative and quantitive evaluation of islets and cell-based screening for new diabetes treatments.

Introduction

Development of an optimal *in vitro* and *ex vivo* analytical tool is very important for understanding the complexity of the physiological and pathophysiological behavior of islets of Langerhans, for both basic science and for the evaluation of new therapeutic compounds. Islets are clusters of 1000–2000 cells (50–400 μm in diameter) found within the pancreas. The majority of these cells are hormone-producing and compromise approximately 2% of the total pancreatic mass. Within each islet, there are mainly heterogeneous populations of alpha and beta-cells, which act to maintain blood glucose homeostasis by responding to and controlling moment-to-moment changes of blood glucose levels through the secretion of glucagon and insulin, respectively. Permanent disruption of this regulatory system consequently results in the onset of diabetes, which is one of the most common metabolic diseases afflicting hundreds of millions of people worldwide.

In vivo, islets experience dynamic changes in their environment and secrete hormones in a biphasic and oscillatory pattern, which is controlled by complex and sequential metabolic events, channel modulation and ion signaling. Traditionally, *in vitro* islet research is carried out using conventional static wells or plates. Secreted total insulin is then further analyzed by biological and biochemical approaches such as ELISA. A dynamic *in vitro* model would be advantageous, as it could more accurately replicate *in vivo* physiological cues and islet physiological activities.

The islet perifusion concept was introduced in the 1970s.[1] Since then, many macro-scale perifusion devices have been developed to understand hormone secretion kinetics and to develop anti-diabetic drugs. However, these devices have many limitations, such as cumbersome operation, limited flow control, inadequate mimicking of *in vivo* microenvironment, and a lack of integration with conventional analytical techniques. These challenges have limited the broad adoption of macro-scale perifusion devices despite their obvious advantages over static conditions.[2]

In the last decade or so, microfluidic technology has emerged as a valuable tool for islet studies, mainly due to its versatility, minimal consumption of reagents and enhanced efficiency.[3–8] Its small scale also allows for the leveraging of microscale flow phenomena (laminar flow and rapid diffusion), both of which are critical for understanding hormone secretion kinetics. In addition, microfluidics allows for easier integration of new experimental modalities, which can integrate multimodal assays and multiple tasking into a single device and improve experimental throughputs.

In our previous studies, we have developed several microfluidic devices mainly used as islet microperifusion devices. These devices have been successfully integrated with live-cell

[a] *Department of Surgery/Transplant, University of Illinois at Chicago, Chicago, IL, 60612 USA. E-mail: jober@uic.edu, wangy@uic.edu*
[b] *Department of Bioengineering, University of Illinois at Chicago, Chicago, IL, 60607 USA*
[c] *Department of Electroengineering, Northern Illinois University, Chicago, IL, 60115 USA*

† Electronic supplementary information (ESI) available: SIV1: islet loading. SIV2: particle tracing simulation. SIV3: solution exchange using fluorescein solutions. See DOI: 10.1039/c5lc01173f

multimodal imaging methods in determining islet cell physiological behavior.[9–13] One of the major challenges of these devices is the limited number of islets that can be assessed in a single device. Another challenge is the inability to satisfactorily assess the heterogeneous property of individual islets, especially when testing a large quantity of islets simultaneously, as data are often averaged from islet populations. Examination of heterogeneous properties at the individual islet level often provides more detailed physiological or pathophysiological information than averaging-based population methodologies. For example, it will enable better understanding of human islet functionality from a reasonable sample size and could provide a better predictive value for islet transplant outcomes if many individual islets can be individually assessed instead of averaging a bulk response.

In this report, our aim is to develop a microfluidic islet array based on the hydrodynamic trapping principle, for investigating the complexity of physiological or pathophysiological behavior of individual islets in a larger population. Furthermore, we aim to explore the feasibility of array-based cellular analysis to provide more informative data on islets and to act as a high content screen platform.

Experiments

Design principle and device configuration

The array device utilizes the hydrodynamic trapping principle to immobilize individual islets in traps (Fig. 1). The principle was first described in 2008 by Tan and Takeuchi.[14] and again was applied by others.[15,16] We have used the same principle to design a microfluidic device for encapsulated islets.[15] However, designing an islet array using the same principle was a challenge and it required careful design consideration due to the various sizes of islets. This was not an issue for microcapsules, since they are uniform in size.

Calculation of pressure drop for designing microchannel geometry

In order to optimize the trapping efficacy for islets, flow resistance of the U-cup and the loop channel was calculated using the Darcy–Weisbach equation, which was further modified by Poiseuille's Law for a rectangular channel. More details can be found in the ESI.†

Computer simulation

To better understand the flow characteristics around the microfluidic traps and determine the optimal parameters for microfluidic channel design, computational fluid dynamics analysis was carried out using COMSOL 4.4 (COMSOL Multiphysics, Sweden). The results of the fluid flow simulation are discussed in the ESI.†

Device fabrication

The microfluidic array device was fabricated using standard soft lithography techniques as described previously.[9,10] Details of the device fabrication are provided in the ESI.†

Human and mouse islet isolation and hypoxia treatment

Human pancreata were obtained from organ procurement organizations following formal research consent. Islet isolation, purification, and culture were performed as previously described;[16,17] details are depicted in the ESI.† Mouse islet isolations were performed as previously described;[18] details are depicted in the ESI.†

Human islet hypoxia was achieved by pelleting. In brief, 2000 IEq of human islets were transferred into a 1.5 mL Eppendorf tube containing 1 mL of culture media and then pelleted by brief centrifugation of the cells for 5 s at a speed of 1000 rpm.

Islet loading, stimulation, and retrieval

In order to achieve high trapping efficacy with a minimal shear force exerted on the islets, both islets and solutions containing insulin secretagogues were delivered into the device using a hydrostatic pressure-driven method. Details of this method are described and illustrated in the ESI.†

Real-time fluorescence imaging

Imaging experiments were performed according to our previously established protocol.[9,19] Detailed imaging methods and protocols are provided in the ESI.†

Confocal imaging and data analysis

Islets were stained with CellTracker Green CMFDA for live cells (Invitrogen, USA), and propidium iodide (PI, Invitrogen, USA) for dead cells. Details of the dye incubation and confocal microscopy protocol are described in the ESI.†

Quantitative live/dead assay of human islets was also performed using ImageJ software (National Institutes of Health). To determine the level of fluorescence intensity in a given region(s) (*e.g.* islet), the regions of interest were selected using the drawing/selection tools in the ImageJ software. The selected areas were then analyzed for areas, integrated density and mean gray value. A region next to the islet that had no fluorescence was also selected as a background. The following formula was used to calculate the corrected total cell fluorescence (CTCF): CTCF = integrated density – (area of a selected islet × mean fluorescence of background readings).[20]

Statistics

Data were expressed as mean ± SD. Unpaired student's t test was performed to compare the group difference. $P < 0.05$ was considered statistically significant.

Results and discussion

1. Comparison between the perifusion chamber device and the islet array device

In order to demonstrate the superior characteristics of the microfluidic array design (Fig. 2A), we compared it to a

previously designed three-layer microfluidic perifusion device (Fig. 2B),[9,19] in which the media used perifusate islets through a perifusion chamber.

The top-layer of the perifusion device has an inlet and an outlet with dimensions of 20 mm × 2 mm × 500 μm. The perifusion chamber is 7 mm in diameter and 3 mm in depth with a total liquid volume of 115 μL. The bottom layer consists of an array of tiny circular wells (500 μm in diameter and 150 μm in depth) for islet immobilization (Fig. 2B). The array of 500 μm wide by 100 μm deep circular wells has been proven to be quite effective for islet immobilization up to a flow rate of 1.0 ml min^{-1}, with minimal physical stress; however, efficient interaction of islets sitting in the circular wells with the microenvironment is dependent on flow dynamics in the perifusion chamber. Since the perifusion chamber is relatively large and falls in the macroscale category, effective mixing and diffusion becomes challenging, especially at a lower flow rate. On the other hand, a higher flow rate (> 2.0 ml min^{-1}) may cause islets to disgorge from the circular wells.

Microfluidic systems are characterized by low Reynolds numbers and the absence of turbulent flow to enhance mixing; therefore, simple diffusion adequately describes the transport of diffusive species within a microchannel. Simple or Fickian diffusion is described by:

$$J = -D\frac{\partial C}{\partial V}$$

where J is the diffusive flux, D is the coefficient of diffusion for a chemical species in a given medium and C is the concentration of the chemical species. The relationship $\chi^2 = 2Dt$ describes the mean square displacement of a particle in relation to time lapsed in the system. As time depends on the square of displacement, diffusion on the microscale occurs much faster than diffusion on the macroscale. Due to the small size of the islet array device (100 times smaller than the perifusion chamber device) and array format, diffusion and mixing are significantly faster and consequently more effective. Additionally, solution consumption can be reduced significantly during the experimental procedure using the newly designed device we present in this paper. The trapped islets in the array had a direct and complete contact with flow independent of flow rate and the islets remained stable during dynamic perifusion with a minimal movement. The previous perifusion design had a limited range of working flow rates, since a slow flow rate (< 50 μL min^{-1}) prevented efficient mixing, while a higher flow rate (> 2 mL min^{-1}) dislodged many trapped islets. Additionally, the design reduced stimulation/washing times, which minimized shear stresses on the islet cells.

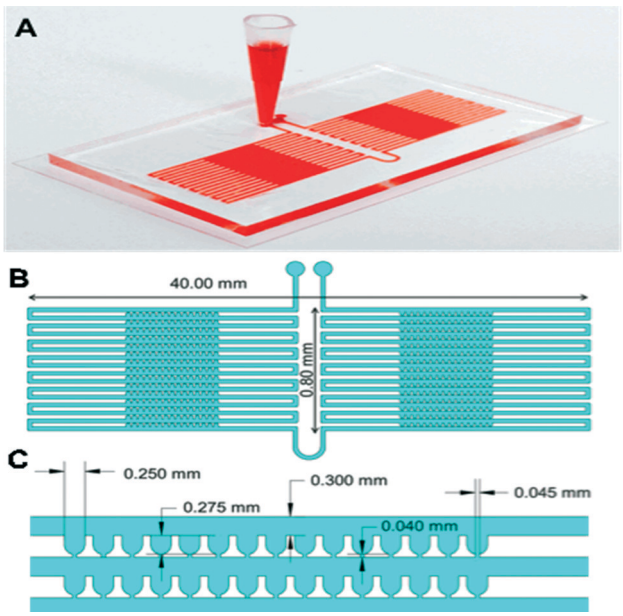

Fig. 1 Microfluidic islet array. (A) Photo image of the microfluidic islet array. (B) Schematic of the microfluidic islet array. (C) Geometrical dimensions of the microfluidic islet array.

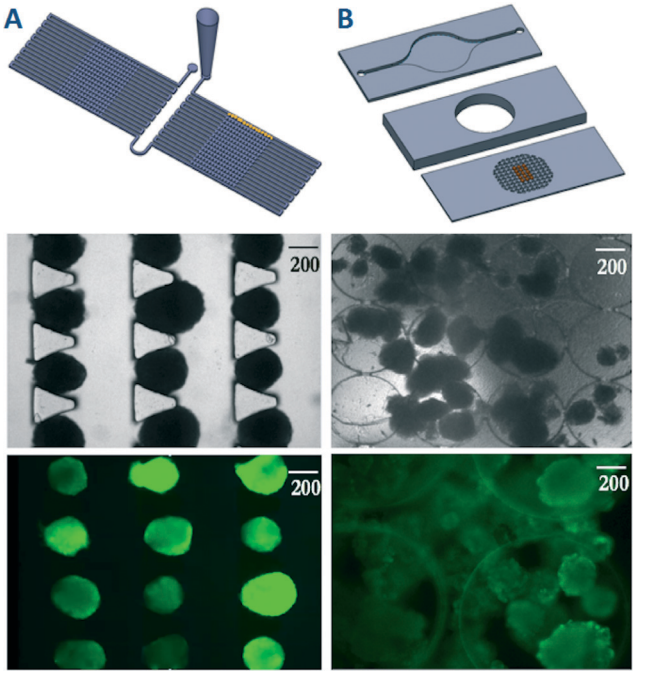

Fig. 2 Microfluidic islet array and microfluidic perifusion device. (A) Schematic of the microfluidic islet array trapped human islets and fluorescence labelled human islets. (B) Schematic of the microfluidic islet perifusion device trapped human islets and fluorescence labelled human islets.

Importantly, the islet array design improved the precision and sensitivity of human islet calcium signaling by effectively detecting subtle changes such as phase 0 (Fig. 3B), which is often not detectable in our previous perifusion based device (Fig. 3A). The glucose-induced phase 0 results from gradual depolarization of a cell membrane and decrease in intracellular calcium. Vanished (non-detectable) phase 0 is often caused by endoplasmic reticulum stress associated with a defect of islet cell function.[21]

Compared to the perifusion chamber design, the human islets in the islet array have superior maximal $[Ca^{2+}]_{glu}$

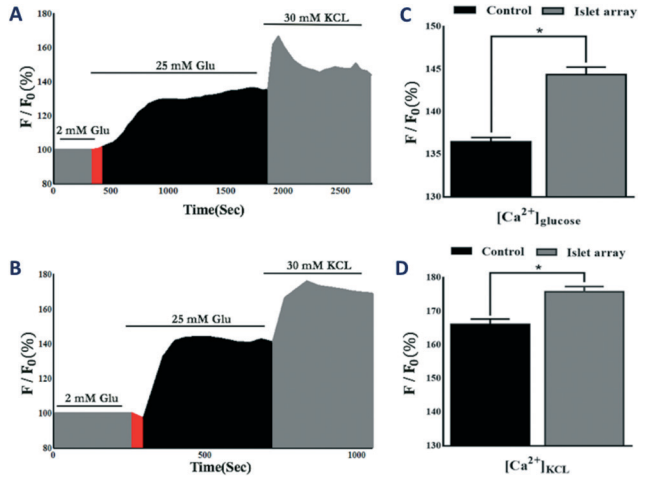

Fig. 3 Comparison of calcium signalling between the perifusion device and the islet array. (A) Calcium profile of human islets trapped in the perifusion device in response to glucose and KCL (n = 3, total of 300 islets). (B) Calcium profile of human islets trapped in the array device in response to glucose and KCL (n = 3, total of 300 islets). (C) Statistical comparison of calcium in response to glucose between the devices. (D) Statistical comparison of calcium in response to KCL between the devices. Red area is indicative of phase 0.

response (144.2% ± 1.73 *vs.* 129.9% ± 2.42; $p < 0.05$) and superior maximal $[Ca^{2+}]_{KCL}$ response (176.2% ± 1.54 *vs.* 166.9% ± 2.13; $p < 0.05$) (Fig. 3C and D). Additionally, the array provided faster transition from phase 0 to phase I (slope: 14.84 *vs.* 2.65).

The islet array increased analytical power, not only by examining 100 islets individually, compared to 50 islets averaged in the perifusion device, but also by efficiently investigating individual islets, which was not achievable in the perifusion chamber as islets often become aggregated or overlaid on each other (Fig. 2B). Lastly, the one-layer array device had minimized dimensions, allowing a much shorter stimulation protocol to achieve comparable results obtained by the perifusion device (s *vs.* min) and consumed a much smaller liquid volume (μL *vs.* mL).

The aforementioned advantages demonstrate that the array can be used as a new gold standard to study islet physiology and therapeutic screening.

2. Optimization of single-islet loading efficiency

To allow high quantity and high-resolution imaging of individual islets in an array, we further characterized the impact of geometries on trapping efficacy. As described previously, an islet, directly prior to entering a trap, experiences forces in two directions: mainstream flow (Q_2) in the loop channel that moves the islet along the loop channel and partial stream flow (Q_1) in the cross-flow channel that pushes the islet into the trapping area. Combined effects of these two flow forces will determine the trapping efficacy of individual islets. We experimentally verified optimal geometry using varying lengths, widths and depths of the trapping site and the loop channel (H), as shown in Fig. 4. When Q_1/Q_2 was equal to 5.5, a high resistance ratio resulted in all traps being occupied, but at the cost of having multiple particles per trap (Fig. 4A). When Q_1/Q_2 was equal to 0.7, the flow going through the trap was not sufficient for optimal loading, resulting in very few traps being occupied (Fig. 4C). By optimizing the fluidic resistance of the cross-flow channel with respect to the resistance of the loop channel (Q_1/Q_2 = 2.8), single particle occupancy on a single trap was achieved (Fig. 4B). At this optimal ratio, 99% ± 2% of the traps are occupied with 95% ± 1% of the occupied traps containing a single particle.

Two additional factors that may influence trapping efficacy are particle concentration and flow rate. Our experience showed that trapping efficacy was independent of initial particle concentration, while particle concentration only affected loading time. For the concentration of 500 islets mL^{-1}, full loading of the array took less than a minute at a flow rate of 50 μL min^{-1} (data not shown). At a lower flow rate, the loading time was longer and the islets tended to settle in the inlet reservoir. For a flow rate above 1 mL min^{-1}, the islets would experience high shear stresses and pressures and sometimes squeeze through the 45 μm narrow gaps, but the time saved was not significant (data not shown). We also observed that an additional benefit of this array design was the sequential capture of incoming islets (SIV1), preventing undesirable islet loss. When a small number of islets enter the islet trap chip, all the islets will be effectively captured. This could be especially useful for precious sample capturing where the tolerance of islet loss is very low.

3. Fluid exchange efficiency

In order to make sure that we achieved a uniform solution distribution and a fast rate of solution exchange in the array channel, a fluorescence intensity experiment using FITC was carried out. The rate of solution exchange was significantly faster (less than 10 second) as a result of a small channel size and volume in comparison to our previous chamber design, which required 3 min to fully exchange.[9] This allows faster stimulation, shorter washing time and improved resolution. More details can be found in the ESI.†

4. Microfluidic array serves as islet cell cytometry

Flow cytometry is a technology that has had a significant impact on basic cell biology and clinical medicine. Its key advantage is that a very large number of particles/cells can be

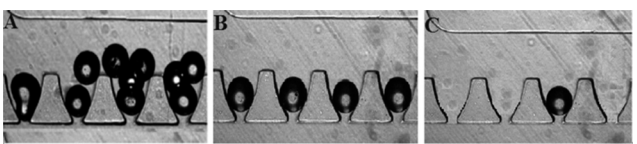

Dimension	W_1	W_2	L_1	L_2	H_1	H_2	Q_1/Q_2
Device A	55	300	50	2000	300	300	5.5
Device B	45	300	55	1500	250	250	2.8
Device C	50	300	55	800	250	250	0.7

Fig. 4 Determination of optimal loading parameter. (A) Loading efficacy at Q_1/Q_2 = 5.5. (B) Loading efficacy at Q_1/Q_2 = 2.8. (C) Loading efficacy at Q_1/Q_2 = 0.7.

evaluated individually in a very fast manner, allowing accurate single- or multi-parameter measurements of particle/cell properties and separation of a single particle/cell physically or biologically from a mixed population to study heterogeneous populations and classifications of subpopulations. Today's instruments have a capacity to measure almost all types of single cells; however, no such instrument for islets has been reported yet. Islets consist of a cluster of approximately 1000–2000 single cells and function as a basic unit. Therefore, it is more physiologically relevant to analyze intact islets rather than dissociated islet single cells. Another advantage over flow cytometry is that our microfluidic chip coupled with real-time microscopy allows tracking of dynamic behavior of hundreds of islets, which cannot be measured by traditional flow cytometry. With our chip, we are able to collect data on behavior of 300 individual islets at different time points under different stimulations, thereby increasing the experimental throughput.

This microfluidic array can successfully capture and immobilize a large number of islets. With a low magnification optical objective, such as a 10× objective, 5 individual islets can be monitored in a field of view. Assisted by a motorized microcopy stage, we collected and analyzed 100 data points from individual islets with a 100-islet array. It is worth noting that this array could be expanded, as the channel has traps to hold up to 300 particles; however, the first 100 traps were used for this study, as there were limitations with how fast the stage could scan. These limitations could be overcome through the use of advanced stage setups.

4.1 Heterogeneous responses of human and rodent islets in response to secretagogues

Glucose-induced insulin secretion is a complex process controlled by beta-cell metabolic events, electrical activity and ion signalling, and displays biphasic and pulsatile kinetic profiles. In short, glucose metabolism increases ATP production, which consequently closes ATP-sensitive K^+ channels, initiates plasma membrane depolarization and increases $[Ca^{2+}]_i$ *via* voltage-dependent calcium channels. This increase in $[Ca^{2+}]_i$ triggers the fusion of insulin granules with a cell membrane and, subsequently, results in insulin exocytosis. The dynamic visualization of physiological changes in individual islets has clear advantages because it provides detailed spatiotemporal information in a quantified manner. For example, the human islet isolation process for islet transplantation is a very complex and multistep process. Each manipulation step may be stressful and even detrimental to islets. The current standard assay to determine the function and viability of human islets provides limited information on physiological or pathophysiological changes of islets. Using this microfluidic-based islet-trapping array, we can observe individual human islets and focus on several key insulin stimulator-secretion coupling pathways in response to secretagogues.

Variable responding profiles of islet calcium and mitochondrial potential changes are shown in Fig. 5A and C. The human islets displayed variable calcium profiles in response to glucose and KCL (25 mM glucose: 144.2% ± 1.74, max: 149.9%, min: 139.9 %; 30 mM KCL: 176.2 % ± 1.54, max: 179.1%, min: 173.5%) and variable mitochondrial potential changes in response to glucose (25 mM glucose: 71.3% ± 2.02, max: 76.8%, min: 62.3%). The heat map of calcium concentration and mitochondrial potential changes are depicted in Fig. 5B and D and provide far richer sources of data compared to bulk averaging over multiple islets.

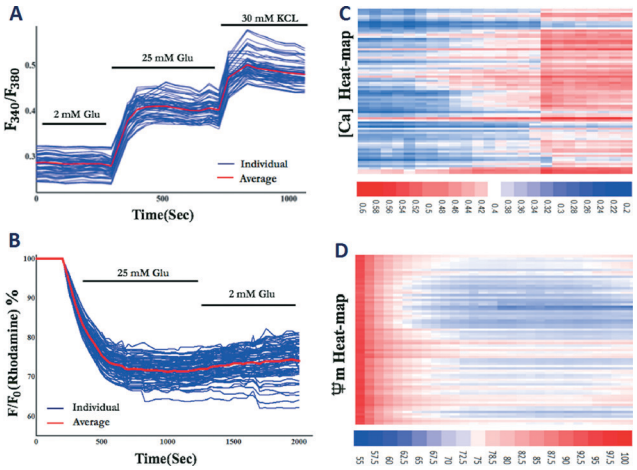

Fig. 5 Variable responding profiles of human islets in response to secretagogues. (A) Calcium signalling in response to 25 mM glucose and 30 mM KCL (n = 3, total of 300 islets). (B) Calcium concentration heat map in response to 25 mM glucose and 30 mM KCL (n = 3, total of 300 islets). (C) Mitochondrial potential changes in response to 25 mM glucose (n = 3, total of 300 islets). (D) Mitochondrial potential change heat map in response to 25 mM glucose (n = 3, total of 300 islets). Information about different response profiles of human and mouse islets in response to varying glucose concentrations and calcium-induced mitochondrial potential oscillation patterns are presented in the ESI† figures.

The microfluidic array clearly provides advantages over population-based approaches by providing more detailed and spatiotemporal analysis of individual islets, not only in a large cell population, but also in varying values (maximal and minimal values) of individual islets, frequencies of responses and percentage response profiles. Additionally, the array may help to identify potential subgroups or sub phenotypes of an islet population, which is critically important for functional characterization of human islets used for islet transplantation and phenotype characterization of beta-cell like stem cells in their differentiation and maturation processes.

Previous studies indicated that glucose-induced cytoplasmic calcium signaling modulates mitochondrial membrane potentials in rodent islets, showing that the increased cytoplasmic calcium depolarizes mitochondrial potentials and subsequently regulates cytoplasmic calcium oscillation and insulin secretion.[22,23] Here, we applied our microfluidic device to test whether our system is capable of observing similar results and to further confirm such results in isolated human islets. Our results obtained using rodent islets showed that increased cytoplasmic calcium induced by 10 mM glucose depolarizes mitochondrial potentials (Fig. 6A), which is similar to previously published data. On the contrary, in the isolated human islets, no obvious mitochondrial potential

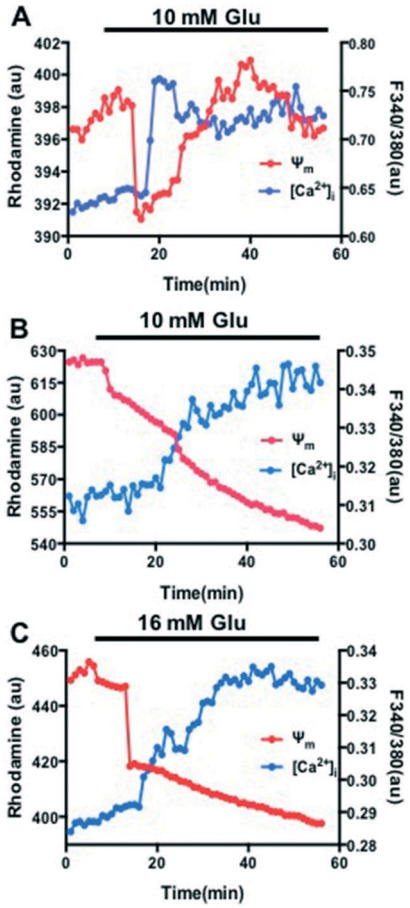

Fig. 6 Spatiotemporal relationship between cytoplasmic calcium and mitochondrial potentials under glucose stimulation. (A) Representative traces of calcium and mitochondrial potentials from mice islets stimulated by 10 mM glucose (n = 20). (B) Representative traces of calcium and mitochondrial potentials from human islets stimulated by 10 mM glucose (n = 15 islets of two preparations). (C) Representative traces of calcium and mitochondrial potentials from human islets stimulated by 16 mM glucose (n = 15 islets of two preparations).

depolarization induced by glucose-increased calcium has been observed under both 10 mM and 16 mM glucose (Fig. 6B and C). The difference between the rodent and the human islets may be related to species difference or low human islet quality, since human islets often have a much longer ischemia time (>8 h) and undergo a harsh isolation process. However, further investigation is needed to clarify underlying causes.

4.2 Islet viability assay

Low islet viability is one of the main obstacles limiting islet transplantation success. There are strong evidences indicating that islet stresses originated at the time of organ procurement, during isolation and in culture have detrimental effects on islet yield and viability.[24] The new microfluidic chip proposed here can be used as a tool to perform high-resolution analysis for islet viability and cell death. Since the trapped islets in the array device are directly located on a thin coverslip (60 × 24 mm and 0.13 mm in thickness), this enables high spatial resolution imaging of islets at a high magnification such as confocal microscopy (Fig. 7). This device also allows us to perform the assessment faster and in a more automated fashion, since the position and location of each trapped islet and the trapping site are known; hence, the imaging process can be performed in an automated way using a motorized stage. Additionally, fluorescence staining and washing processes can be performed on the chip without any difficulty.

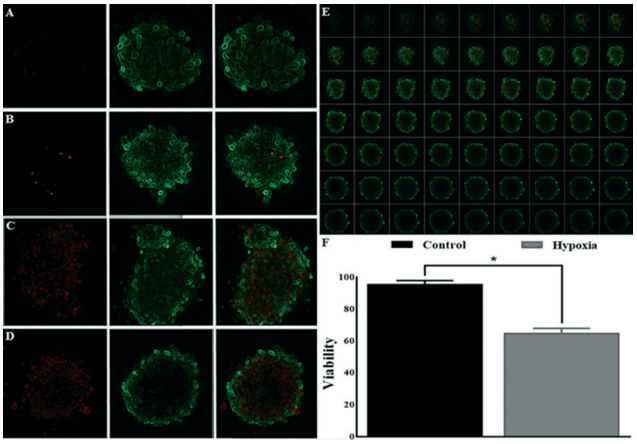

Fig. 7 Confocal imaging and quantification of live cells and dead cells of the human islets in the array. (A and B) Representative images of the control human islets. (C and D) Representative images of the hypoxia-treated human islets. (E) Representative images of a human islet were collected at 10 μm intervals to create a stack in Z axis (63 z-slices recorded with a 20× lens). (F) Statistical analysis of human islet viability from the control islets and the hypoxia-treated islets (n = 3, total of 150 islets; $*p < 0.01$).

Fig. 7 shows the results of the standard CMFDA/PI assay performed on the human islets. Each sample contained 50 islets for each condition. The percentage of viable and dead cell aggregates over the total amount of aggregates was determined by scoring green *versus* red fluorescence using the ImageJ software package as described under the "Experiments" section.

Quantitative comparisons showed that the viability percentages of the control islets and the hypoxia treated islets were 96.1% ± 2.34 and 65.2% ± 3.21, respectively ($p < 0.01$).

The standard islet viability assay using a lower optical objective only assesses the cell viability of islet peripheral layers and surface areas, which often provides limited information of islet viability, since islets are clusters of 1000–2000 single cells with diameters from 50–400 μm. Additionally, the manual approach is highly operator-dependent and subjective. The confocal evaluation of islet viability in the array assisted by an image processing software provides more informative and accurate analysis by assessing each layer of islet cells including the islet core in a large islet population. Importantly, the approach can reduce operator bias.

Conclusions

In this study, we presented a novel microfluidic array based on a hydrodynamic trapping mechanism. The unique feature

of the device is its suitability for high-resolution analysis of individual islets. We have identified key design parameters controlling the trapping efficacy. This work demonstrates the enabling capability of quantitative analysis as islet cytometry that can be readily adopted for studying physiological and pathophysiological properties of islets. In contrast to existing microfluidic perifusion devices, the presented array provides well-controlled flow dynamics with much improved flow exchange, faster flow delivery, a shortened stimulation protocol, and improved assay sensitivity and accuracy. Importantly, it is the first device that has an ability to monitor a large population at the single islet level, which can be very useful for evaluation of human islet function and viability and in screening potential anti-diabetic compounds. In the future, we are planning to further optimize the system for the effective collection of perifusates for hormone measurements.

Acknowledgements

The authors thank the UIC human islet isolation and transplantation program for providing technical support. This work was in part supported by NIH R01 DK091526 (JO, YW), JDRF Microfluidic-Based Functional Facility at UIC, and the Chicago Diabetes Project (CDP).

References

1 P. E. Lacy, M. M. Walker and C. J. Fink, *Diabetes*, 1972, **21**, 987–998.
2 Y. Wang, J. F. Lo, J. E. Mendoza-Elias, A. F. Adewola, T. A. Harvat, K. P. Kinzer, D. Lee, M. Qi, D. T. Eddington and J. Oberholzer, *Bioanalysis*, 2010, **2**, 1729–1744.
3 J. G. Shackman, G. M. Dahlgren, J. L. Peters and R. T. Kennedy, *Lab Chip*, 2005, **5**, 56–63.
4 M. G. Roper, J. G. Shackman, G. M. Dahlgren and R. T. Kennedy, *Anal. Chem.*, 2003, **75**, 4711–4717.
5 J. F. Dishinger, K. R. Reid and R. T. Kennedy, *Anal. Chem.*, 2009, **81**, 3119–3127.
6 J. V. Rocheleau, G. M. Walker, W. S. Head, O. P. McGuinness and D. W. Piston, *Proc. Natl. Acad. Sci. U. S. A.*, 2004, **101**, 12899–12903.
7 P. N. Silva, B. J. Green, S. M. Altamentova and J. V. Rocheleau, *Lab Chip*, 2013, **13**, 4374–4384.
8 D. Chen, W. Du, Y. Liu, W. Liu, A. Kuznetsov, F. E. Mendez, L. H. Philipson and R. F. Ismagilov, *Proc. Natl. Acad. Sci. U. S. A.*, 2008, **105**, 16843–16848.
9 J. S. Mohammed, Y. Wang, T. A. Harvat, J. Oberholzer and D. T. Eddington, *Lab Chip*, 2009, **9**, 97–106.
10 A. F. Adewola, D. Lee, T. Harvat, J. Mohammed, D. T. Eddington, J. Oberholzer and Y. Wang, *Biomed. Microdevices*, 2010, **12**, 409–417.
11 J. F. Lo, Y. Wang, A. Blake, G. Yu, T. A. Harvat, H. Jeon, J. Oberholzer and D. T. Eddington, *Anal. Chem.*, 2012, **84**, 1987–1993.
12 D. Lee, Y. Wang, J. E. Mendoza-Elias, A. F. Adewola, T. A. Harvat, K. Kinzer, D. Gutierrez, M. Qi, D. T. Eddington and J. Oberholzer, *Biomed. Microdevices*, 2012, **14**, 7–16.
13 Y. Wang, D. Lee, L. Zhang, H. Jeon, J. E. Mendoza-Elias, T. A. Harvat, S. Z. Hassan, A. Zhou, D. T. Eddington and J. Oberholzer, *Biomed. Microdevices*, 2012, **14**, 419–426.
14 W. H. Tan and S. Takeuchi, *Lab Chip*, 2008, **8**, 259–266.
15 M. Nourmohammadzadeh, J. F. Lo, M. Bochenek, J. E. Mendoza-Elias, Q. Wang, Z. Li, L. Zeng, M. Qi, D. T. Eddington, J. Oberholzer and Y. Wang, *Anal. Chem.*, 2013, **85**, 11240–11249.
16 M. Qi, B. Barbaro, S. Wang, Y. Wang, M. Hansen and J. Oberholzer, *J. Visualized Exp.*, 2009, **27**, 1125.
17 M. Qi, B. Barbaro, S. Wang, Y. Wang, M. Hansen and J. Oberholzer, *J. Visualized Exp.*, 2009, **27**, 1125.
18 Y. Wang, S. Wang, T. Harvat, K. Kinzer, L. Zhang, F. Feng, M. Qi and J. Oberholzer, *Cell Transplant.*, 2015, **24**, 25–36.
19 A. F. Adewola, D. Lee, T. Harvat, J. Mohammed, D. T. Eddington, J. Oberholzer and Y. Wang, *Biomed. Microdevices*, 2010, **12**, 409–417.
20 R. A. McCloy, S. Rogers, C. E. Caldon, T. Lorca, A. Castro and A. Burgess, *Cell Cycle*, 2014, **13**, 1400–1412.
21 J. F. Worley, 3rd, M. S. McIntyre, B. Spencer, R. J. Mertz, M. W. Roe and I. D. Dukes, *J. Biol. Chem.*, 1994, **269**, 14359–14362.
22 P. Krippeit-Drews, M. Dufer and G. Drews, *Biochem. Biophys. Res. Commun.*, 2000, **267**, 179–183.
23 H. Kindmark, M. Kohler, G. Brown, R. Branstrom, O. Larsson and P. O. Berggren, *J. Biol. Chem.*, 2001, **276**, 34530–34536.
24 C. Ricordi and T. B. Strom, *Nat. Rev. Immunol.*, 2004, **4**, 259–268.

